Rheological and Thermal Properties of Elastomeric Polypropylene

Eric D. Carlson,[†] Mark T. Krejchi,[‡,§] Chirag D. Shah,[‡] Toshitsugu Terakawa,[†,||] Robert M. Waymouth,[*,‡] and Gerald G. Fuller[†]

Department of Chemical Engineering and Department of Chemistry, Stanford University, Stanford, California 94305

Received July 22, 1997; Revised Manuscript Received March 30, 1998

ABSTRACT: The properties of elastomeric polypropylene synthesized from an unbridged metallocene catalyst are investigated by mechanical rheometry, differential scanning calorimetry, and optical depolarization. The material is compositionally heterogeneous in tacticity, and its behavior is compared to that of its solvent fractions. The behavior of elastomeric polypropylene is also compared with tacticity-matched atactic/isotactic homopolymer blends. For T below T_m, mechanical rheometry shows that elastomeric polypropylene forms a more constrained network than tacticity-matched homopolymer blends. Differential scanning calorimetry reveals that the elastomeric samples crystallize at a lower temperature than blends composed of the same isotactic content. Depolarization studies show similar transitions but reveal the presence of an additional slower time scale involved with crystallizing the elastomeric sample. Data are consistent with the presumed atactic/isotactic multiblock microstructure of elastomeric polypropylene.

Introduction

Polypropylene composed of blocks of isotactic and atactic stereosequences form an interesting family of thermoplastic elastomers.[1] Elastomeric polypropylene, or rubbery polypropylene, is an unusual elastomer in that it is derived from a single monomer unit. The stereoregular structure of isotactic polypropylene enables it to form helices that can pack into crystals. Atactic polypropylene is stereoirregular and is consequently amorphous at all temperatures. The thermoplastic elastomeric behavior of rubbery polypropylene is proposed to arise from amorphous atactic stereosequences that are physically cross-linked by isotactic polypropylene crystallites, as shown in the idealized representation in Figure 1. Rubbery polypropylene was first produced by Natta, who interpreted the elastomeric properties in terms of a stereoblock structure of crystallizable isotactic blocks and noncrystallizable atactic blocks.[2−4]

Elastomeric polypropylene can be prepared by several approaches, including heterogeneous Ziegler−Natta catalysts,[5,6] Zr and Ti alkyls on alumina supports,[7−9] and stereorigid metallocene catalysts.[10−12] We have recently reported the synthesis of elastomeric polypropylene with metallocene catalysts derived from bis(2-phenylindenyl)zirconium dichlorides.[13] These catalysts were designed to interconvert between chiral, isospecific and achiral, aspecific forms to produce blocks of isotactic and atactic stereosequences. These catalysts are capable of synthesizing polypropylenes with a wide range of tacticities, from highly atactic samples to moderately isotactic, elastomeric samples to highly isotactic samples.

In this study, we examine the physical behavior of an elastomeric polypropylene sample synthesized with a metallocene catalyst derived from bis(2-phenylindenyl)zirconium dichloride. Fractionation of the elastomeric polypropylene was carried out and the behavior of the elastomeric polypropylene and its fractions is compared to that of tacticity-matched homopolymer blends. Mechanical rheometry is used to contrast the viscoelastic response of elastomeric polypropylene with the viscoelastic behavior of the blends. Differential scanning calorimetry (DSC) and optical depolarization studies reveal that elastomeric polypropylene exhibits slower crystallization kinetics than corresponding homopolymer blends.

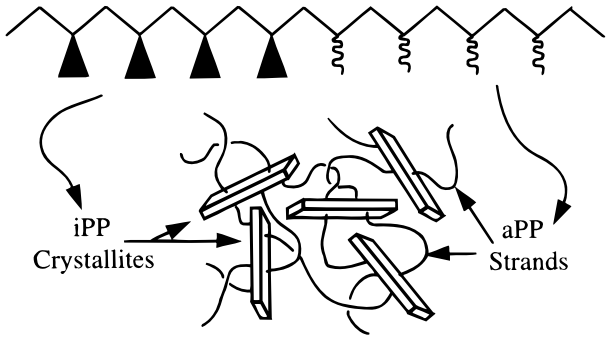

Figure 1. Idealized representation of stereoblock polypropylene microstructure. Isotactic polypropylene blocks have the ability to crystallize and physically cross-link amorphous atactic polypropylene segments due to connectivity between blocks.

Experimental Section

Synthesis. An elastomeric polypropylene sample (ePP) was prepared at Amoco Chemical Co. using an unbridged metallocene catalyst derived from bis(2-phenylindenyl)zirconium dichloride. The methylaluminoxane (MAO) cocatalyst (Akzo type 4A, dried under vacuum at 60°) (2 g/10 mL) and bis(2-phenylindenyl)zirconium dichloride catalyst precursor (0.04 g/10 mL) solutions were separately prepared in toluene. A 2-gallon autoclave was charged with liquid propylene at 20 °C. The catalyst and catalyst precursor solutions were premixed and allowed to age for 30 min at room temperature. The catalyst solution was injected into the autoclave with

* To whom correspondence to be addressed.
[†] Department of Chemical Engineering.
[‡] Department of Chemistry.
[§] Present address: Wilsonart, 505 South General Bruce Drive, Temple, TX 76503.
[||] Present address: Daicel Chemical, Osaka, Japan.

S0024-9297(97)01106-6 CCC: $15.00
Published on Web 07/21/1998

nitrogen, and polymerization was conducted at 23 °C. After 2 h, the reaction mixture was pressurized into a solution of hexane and methanol to terminate polymerization. The solvent and unreacted propylene monomer were removed and the crude reactor crum was dried at 50 °C in vacuo. The yield for the polymerization under these conditions was approximately 130 g.

Atactic polypropylene (aPP) was prepared with a toluene solution of (2-phenylindene)hafnium dichloride and MAO. In a drybox, a 300 mL Parr reactor was loaded with 290 mg of MAO cocatalyst (Akzo type 4a, dried under vacuum at 60 °C). A 50 mL injection tube was loaded with a toluene solution of (2-phenylindenyl)hafnium dichloride (3 mg/10 mL). The catalyst was injected into a reactor containing 80 mL of toluene that had been preequilibrated with 100 psig polypropylene. The reactor temperature was maintained at 20 °C throughout the course of the reaction. After 1 h, the reaction was quenched with methanol (approximately 10 mL). The polymer was precipitated from solution over several hours. The yield for the polymerization under these conditions was approximately 23 g. aPP was found to have a ^{13}C NMR [mmmm] = 0.10, an IR $A_{998}/A_{974} = 0.22$, and a $M_w = 496\,000$ ($M_w/M_n = 2.1$).

A sample of Amoco 4018 isotactic polypropylene (iPP290) was obtained from Amoco Chemical Co.. iPP290 has an [mmmm] = 0.91, an $A_{998}/A_{974} = 0.97$, and a $M_w = 290\,000$ ($M_w/M_n = 7.0$). Regioerror densities were determined by quantitative ^{13}C NMR measurements and are reported in terms of 2,1 erythro regioerrors (%2,1E), 2,1 threo regioerrors (%2,1T), and 1,3 regioerrors (%1,3). iPP290 contains no measurable regioerrors. Additional isotactic polypropylenes (iPP41, iPP16) were synthesized with a metallocene catalyst derived from ethylenebis(indenyl)zirconium dichloride. For iPP41, a Parr reactor was charged with a MAO solution in toluene (Akzo type 4a, dried under vacuum at 60 °C) (280 mg/75 mL). An injection tube was charged with a toluene solution of the ethylenebis(indenyl) zirconium dichloride (2 mg/20 mL). The reactor was placed under 3.4 atm propylene and held for 5 min to equilibrate. The catalyst solution was injected with nitrogen. After an initial overshoot in temperature, the reaction was carried out at 25 °C. After 1 h, the reaction was quenched with methanol (10 mL). The polymer was precipitated and dried in vacuo at 60 °C. Polymerization yielded approximately 30 g of iPP41, which has an [mmmm] = 0.86, an $A_{998}/A_{974} = 0.81$, and a $M_w = 41\,000$ ($M_w/M_n = 2.4$). iPP41 contains 1.1 mol % total regioerrors (%2,1E = 0.6, %2,1T = 0.3, and %1,3 = 0.2). For iPP16, 10 mg of ethylenebis(indenyl) zirconium dichloride was dissolved in 5 mL of a 30% MAO solution of toluene. Then 2 mL of this solution was added to a saturated solution of propylene in toluene (2.1 atm, 220 mL of toluene, 20 °C). After 1 h, the polymerization was quenched with methanol, precipitated, and dried in vacuo at 60 °C. The polymerization yielded approximately 31 g of iPP16, which has an [mmmm] = 0.84, an $A_{998}/A_{974} = 0.78$, and a $M_w = 16\,000$ ($M_w/M_n = 2.1$). iPP16 contains 1.2 mol % total regioerrors (%2,1E = 0.5, %2,1T = 0.4, and %1,3 = 0.3). These quantitative regioerror density measurements for the isotactic homopolymers compare favorably with those of Galante et al.[14]

Polymer purification is conducted in a 500 mL round-bottom flask charged with xylenes (300 mL) and 2,6-di-*tert*-butyl-4-methylphenol (1 g). The crude reactor crum (2 g) was dissolved at reflux under nitrogen. The polymer solution was hot filtered over Celite by vacuum and precipitated into acidified methanol (1% HCl) with vigorous stirring. The rubbery white precipitate was frozen in liquid nitrogen, ground, and washed with acidified methanol (100 mL, 10% HCl). The polymer was dried overnight at 60 °C in vacuo.

The elastomeric polypropylene samples were fractionated[15] by successive extraction with ether and heptane under a nitrogen blanket at the boiling point of the solvent. The extracted polymer was recovered by evaporation of the solvent (60 °C in vacuo).

Homopolymer blends were made to match the isotactic pentad content of the elastomeric polypropylene. A blend of aPP and iPP290 (B290) was prepared by dissolving 0.82 g of iPP290 and 2.18 g of aPP in boiling xylene. A blend of aPP and iPP41 (B41) was prepared by dissolving 0.89 g of iPP41 and 2.11 g of aPP in boiling xylene. A blend of aPP and iPP16 (B16) was prepared by dissolving 0.30 g of iPP16 and 0.70 g of aPP in boiling xylene. Each blend was reprecipitated with the addition of acidified methanol (10% HCl). The residue was filtered and dried at 60 °C in vacuo.

NMR. Solution ^{13}C NMR analysis was performed at 100 °C using a Varian Inova-300 NMR spectrometer operating at 75 MHz on polymer samples dissolved in 1,2-dichloroethane-d_2 (10 wt %). Qualitative measurements were recorded using a spectral and pulse width of 7500 Hz and 28°, respectively, with at least 1000 transients. Broadband decoupling was achieved with the Waltz sequence. Quantitative spectra were acquired using pw = pw90 with at least 3000 transients and a 20 s delay between pulses. Decoupling was always on during acquisition so the nuclear Overhauser enhancement was present. Regioerror concentrations were calculated by using the method outlined by Resconi et al.[16]

IR. Infrared analysis was performed using a Perkin-Elmer 1600 series FT-infrared spectrometer. Pressed polymer films were held at room temperature for 10 h prior to analysis. The films were scanned from 1600 to 450 cm^{-1} with a resolution of 2 cm^{-1}.

GPC. Molecular weight characterization was carried out at Amoco Chemical Co. on a Walters 150C in trichlorobenzene at 145 °C and are referenced against polypropylene standards.

Rheometry. Dynamic mechanical measurements were carried out on a Rheometrics dynamic analyzer (RDA II) using parallel plate geometry. Samples were heated and pressed in the rheometer under a N_2 environment at 200 °C and held for 10 min to erase all thermal history. Samples were then cooled at 20 °C/min to 25 °C, and held for 12 h to provide a common thermal history for all samples. Frequency sweeps were performed from 0.05 to 100 rad/s on 25 mm parallel plates at 0.5% strain. Sweeps were carried out at various temperatures across the DSC heating profile from 25 to 200 °C.

DSC. Calorimetric measurements were carried out on a Perkin-Elmer DSC7 differential scanning calorimeter (DSC). To erase any thermal history, samples were held at 200 °C for 10 min. Crystallization temperatures (T_c) and the enthalpy of crystallization (ΔH_c) were determined by cooling studies in which samples were cooled from 200 °C at 20 °C/min to 25 °C. The melt temperature (T_m) and heat of fusion (ΔH_f) were measured by initially treating the samples in the same manner as the cooling studies, immediately quenching to the samples −50 °C, and then heating the samples to 200 °C at 20 °C/min.

Optical Depolarization. Depolarization studies were carried out on polymer samples pressed between microscope slides under constant load (∼100 g/in.^{2}) at ∼170 °C in vacuo. The prepared slides were placed in a Mettler hot stage positioned between crossed polarizers. Light was provided by a Melles Griot HeNe laser and collected with a photodiode detector. Samples were heated to 200 °C and held for 10 min to erase thermal history. To examine the crystallization behavior, samples were cooled from 200 °C to 25 °C at 10 °C/min. The melting behavior was probed by initially treating the samples as in the cooling study and then immediately heating the samples to 200 °C at 10 °C/min. The intensity of light transmitted through a birefringent sample of arbitrary orientation positioned between crossed polarizers is given by the following expression:[17]

$$I = \frac{I_o}{8}\sin^2(2\theta)\left[\frac{2\pi d\Delta n'}{\lambda}\right]^2 \qquad (1)$$

where I is the transmitted intensity, I_o is the incident intensity, θ is the angle between the initial polarizer and the orientation of the birefringent species in the plane perpendicular to the transmitted beam, d is the sample thickness, λ is the wave-

Table 1. ^{13}C NMR Pentad Distributions

sample	[mmmm]	[mmmr]	[rmmr]	[mmrr]	[rmrr] + [mmrm]	[mrmr]	[rrrr]	[mrrr]	[mrrm]
ePP	0.32	0.15	0.04	0.10	0.18	0.09	0.02	0.05	0.05
ES	0.18	0.16	0.06	0.12	0.22	0.11	0.03	0.07	0.05
HS	0.33	0.16	0.05	0.11	0.17	0.08	0.02	0.05	0.05
HI	0.51	0.12	0.03	0.07	0.13	0.06	0.01	0.04	0.04
aPP	0.10	0.20	0.07	0.16	0.28	0.07	0.03	0.07	0.01
iPP290	0.91	0.04	0.01	0.02		0.01		0.01	
iPP41	0.86	0.07		0.05					0.02
iPP16	0.84	0.08		0.06					0.02
B270	0.32	0.16	0.06	0.12	0.20	0.06	0.02	0.05	0.01
B41	0.33	0.13	0.04	0.11	0.18	0.09	0.02	0.07	0.03
B16	0.30	0.12	0.05	0.11	0.18	0.09	0.03	0.07	0.04

Table 2. Microstructural Characterization

sample	wt % ePP	[mmmm]	A_{998}/A_{974}	%2,1E (mol %)	%2,1T (mol %)	%1,3 (mol %)	total regioerrors (mol %)	$10^{-3}M_w$	M_w/M_n
ePP	100	0.32	0.33					455	2.7
ES	36	0.18	0.19					339	2.5
HS	43	0.33	0.33					367	2.4
HI	21	0.51	0.68					598	3.1
aPP		0.10	0.22					496	2.1
iPP290		0.92	0.97	0	0	0	0.0	290	7.0
iPP41		0.85	0.81	0.6	0.3	0.2	1.1	41.4	2.4
iPP16		0.84	0.78	0.5	0.4	0.3	1.2	15.9	2.1
B290 (iPP290/aPP)		0.32	0.38	(0/−)	(0/−)	(0/−)	(0/−)	(290/496)	
B41 (iPP41/aPP)		0.33	0.43	(1.1/−)	(1.1/−)	(1.1/−)	(1.1/−)	(41.4/496)	
B16 (iPP16/aPP)		0.30	0.39	(1.1/−)	(1.1/−)	(1.1/−)	(1.2/−)	(15.9/496)	

length of light, and $\Delta n'$ is the birefringence. The depolarization, D, is thus taken to be

$$D \propto \frac{\sqrt{I}}{d} \tag{2}$$

Results and Discussion

Sample Preparation and Microstructural Characterization. An unbridged metallocene catalyst derived from bis(2-phenylindene)zirconium dichloride was used to produce an elastomeric polypropylene sample (ePP) at room temperature in liquid propylene. Polymer microstructures were probed by ^{13}C NMR[18−21] and are summarized in Table 1. The fraction of isotactic pentads, [mmmm], is a measurement of a sample's isotacticity. The ePP sample has an [mmmm] = 0.32. Microstructures are also measured in terms of the IR index = A_{998}/A_{974}, which indicates the ratio of helical segments to nonhelical segments.[22−24] The ePP sample has an $A_{998}/A_{974} = 0.33$, which correlates well with the [mmmm] value. GPC measurements show that ePP has an $M_w = 455\,000$ and a $M_w/M_n = 2.7$.

The elastomeric polypropylene ePP can be fractionated by successive extractions into boiling diethyl ether and heptane. Fractionation of ePP yields 36% of an ether-soluble fraction (ES), 43% of a heptane-soluble fraction (HS), and 21% of a heptane-insoluble fraction (HI). The microstructure and properties of the fractions are distinct. The ES has a low isotacticity with an [mmmm] = 0.18. The HS has an [mmmm] = 0.33, matching that of the parent ePP sample. The HI has an [mmmm] = 0.51. The full pentad distributions are included in Table 1. IR measurements correlate with the [mmmm] pentad measurements of isotacticity. The ES, HS, and HI have an $A_{998}/A_{974} = 0.19$, 0.33, and 0.68, respectively. These samples also differ in molecular weight. The ES fraction has the lowest $M_w = 339\,000$ ($M_w/M_n = 2.5$), the HS fraction has an $M_w = 367\,000$ ($M_w/M_n = 2.4$), and the HI fraction has a higher $M_w = 598\,000$ ($M_w/M_n = 3.1$). A summary of NMR, IR, and GPC microstructural results for ePP and its solvent fractions is included in Table 2.

The compositional heterogeneity of ePP prompted us to compare the properties of this material and its fractions to atactic/isotactic homopolymer blends of similar composition. These studies were initiated in an attempt to investigate the importance of segmental connectivity as well as to illuminate the role that a particular fraction or combination of fractions plays in the rheology or crystallization behavior of the parent sample.

An atactic polypropylene homopolymer (aPP) and three isotactic polypropylene homopolymers (iPP290, iPP41, and iPP16) differing in M_w, stereoregularity, and regioerror concentration were used in this study to create three blends that mimic the average microstructure of the ePP sample ([mmmm] = approximately 0.30). The characterization of the homopolymers are summarized in the Experimental Section. The full pentad distributions for all the homopolymers and blends are included in Table 1. Table 2 includes a summary of the [mmmm], A_{998}/A_{974}, regioerrors, and molecular weight values for the homopolymers and blends.

Mechanical Rheology. Small amplitude, oscillatory, mechanical rheometry was used to compare the elastic and viscous responses of the elastomeric polypropylenes[25] and the atactic/isotactic blends. The use of a parallel plate rheometer allows the application a controlled shear flow to the sample across a wide temperature range. As it is generally infeasible to access all frequencies of interest, the principle of time−temperature superposition is used to probe either very high or very low frequencies.[26] The phenomenon of crystallization-induced gelation of thermoplastic elastomeric polypropylene has been studied in detail,[10,27] and as isotactic polypropylene sequences crystallize or melt, time−temperature superposition is expected to break down. The extent of network formation is shown by plotting the storage and loss moduli collected at various stages of melting against shifted frequency to see where time−temperature superposition fails. In cases where

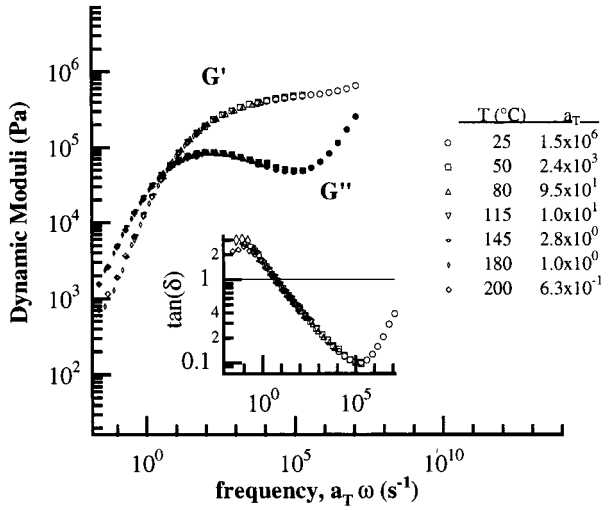

Figure 2. Master curve for atactic sample aPP with dynamic moduli plotted against shifted frequency (T_{ref} = 180 °C). The inset displays the master curve of tan(δ) plotted against shifted frequency. Data points indicate every fifth point.

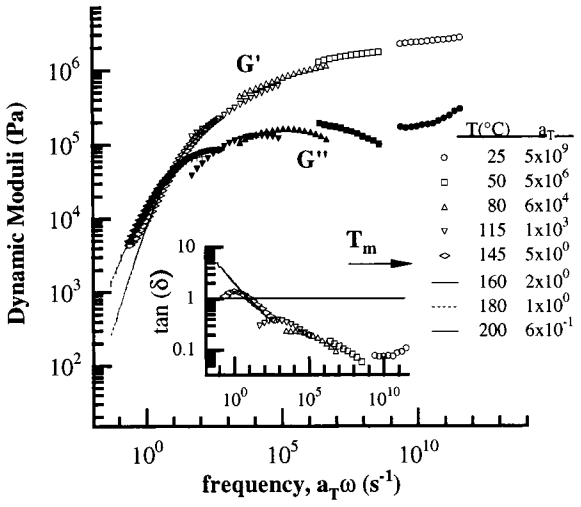

Figure 3. Quasi-master curve for elastomeric homopolymer polypropylene (ePP) with dynamic moduli plotted against shifted frequency (T_{ref} = 180 °C). The inset displays the master curve of tan(δ) plotted against shifted frequency. Data points indicate every fifth point.

isotactic segments are able to crystallize and time−temperature superposition fails, such plots will be referred to as quasi-master curves.

Figure 2 contains the master curve for the atactic homopolymer aPP (T_{ref} = 180 °C), where the open symbols represent the storage modulus, G', and the closed symbols represent the loss modulus, G''. The data are typical for an amorphous, entangled polymer melt. These moduli superimpose extremely well across the temperature and frequency range probed. G'' dominates at frequencies below $\omega_{cross} = 5.0\ s^{-1}$, and the polymer is able to relax with an approach to terminal behavior. Relaxation is inhibited by chain entanglements at frequencies above ω_{cross}, and aPP exhibits an extended rubbery plateau before entering a transition to glasslike behavior at high frequencies. The entanglement molecular weight, M_e, can be calculated from the plateau modulus, G_N°, using the following relation:

$$G_N^\circ = \frac{\rho RT}{M_e} \tag{3}$$

Here, ρ is the polymer density (860 kg/m^3)[28] and RT is the energy stored in a mole of polymer strands. Using the value of G' at the inflection point for G_N° (5.0×10^5 Pa), the calculated entanglement molecular weight for aPP is 4300, which is equivalent to 105 monomers between entanglements. Values for M_e in the literature range from 3500 to 4500.[28]

Figure 3 contains the quasi-master curve for ePP. In contrast to the amorphous polymer aPP, only the ePP moduli collected at temperatures above 150 °C superimpose (solid curves). Data collected at temperatures below 150 °C (individual symbols) are discontinuous when attempts are made at time−temperature superposition. At these lower temperatures ePP behaves as an elastomer that does not flow or relax even at very slow frequencies. This can be more clearly seen in the inset to Figure 3, which contains tan(δ) plotted against shifted frequency, where tan(δ) = G''/G'. Complete relaxation only occurs when the viscous modulus dominates and tan(δ) > 1.0. As the frequency is decreased, tan(δ) exhibits maxima that are less than 1.0, showing that the elastic modulus dominates in this temperature range and continues to increase in relative importance as the frequency is decreased.

Estimates for the amorphous block length in an atactic/isotactic model of elastomeric polypropylenes have previously been derived from the plateau modulus G_N° and eq 3.[10] Using the plateau modulus at 25 °C for ePP (2.4×10^6 Pa) a molecular weight between point constraints (M_{pc}) of 900 can be estimated. This means that ePP has an average amorphous block length of 21 monomers. It should be noted that eq 3 assumes that the network constraints are point restrictions whose locations deform affinely in a flow field. Crystallite structures probably do not deform affinely, thus crystallite tie points may act as a filler in the polymer system. Several empirical relations have been proposed to account for the influence of particulate fillers on polymer moduli.[26] It has been shown that even in a Newtonian fluid the presence of hard spheres resists the extensional component and leads to an increase in the stress.[29] For noninteracting, rigid fillers, the polymer modulus G has been found to increase with the filler volume fraction ϕ:[26]

$$\frac{G}{G_o} = \left[1 + \frac{1.25\phi}{(1 - \phi/\phi_m)}\right]^2 \tag{4}$$

where G_o is the modulus of the unfilled polymer and ϕ_m is the maximum volume fraction corresponding to close packing (approximately 0.75). DSC measurements, discussed in detail below, show that ePP at T = 25 °C is 12.4% crystalline. Assuming noninteracting ePP crystallites and taking $\phi = 0.124$, eq 4 yields a $G/G_o = 1.4$. Equation 3 shows that increases in G_N° lead to decreases in the M_{pc}. Thus, the nondeforming filler acts to shorten the length of chains between equivalent point constraints. Different assumptions about the interactions and geometry of the crystallites would lead to a different predicted filler effect on the modulus, thus the length of the amorphous segment is a nontrivial quantity to estimate from these experiments. To separate the effect of physical cross-links and crystallite fillers, the behavior of ePP is compared with that of a tacticity-matched atactic/isotactic homopolymer in which there is no segmental connectivity to create physical cross-links.

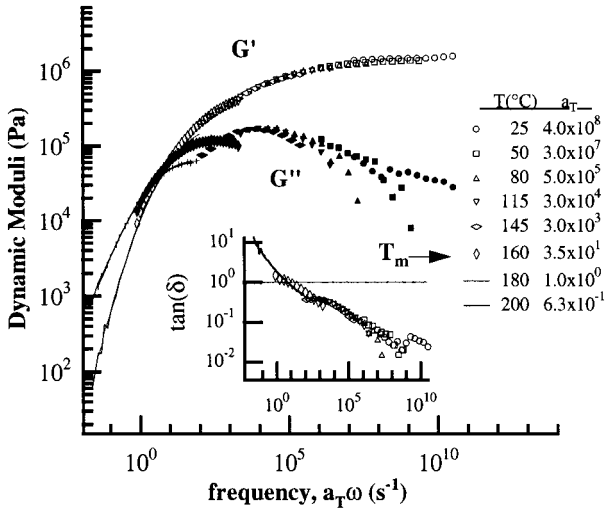

Figure 4. Quasi-master curve for atactic/isotactic blend sample B290 with dynamic moduli plotted against shifted frequency (T_{ref} = 180 °C). The inset displays the master curve of tan(δ) plotted against shifted frequency. Data points indicate every fifth point.

Figure 4 contains the quasi-master curve for the atactic/isotactic blend B290 (T_{ref} = 180 °C). Data collected at 25, 50, 80, 115, and 145 °C (indicated by individual symbols) show well-behaved time−temperature superposition. Data from 180 and 200 °C (indicated by solid lines) also superimpose well and show an approach to flow behavior at frequencies below an ω_{cross} of 11.0 s^{-1}. Data collected at 160 °C do not superimpose with either the low-temperature or the high temperature data. The moduli measured for B290 over the lower temperature range also do not contain a crossover frequency, nor do they suggest the existence of a crossover at extrapolated lower frequencies, suggesting that this system does not relax on these time scales. This can be more clearly seen in the inset to Figure 4, which contains tan(δ) plotted against shifted frequency. Recall complete relaxation occurs when tan(δ) > 1.0. B290 data at 115 and 145 °C contain local maxima in tan(δ) that are less than 1.0, showing that the elastic modulus dominates in this temperature range and continues to increase in relative importance as the frequency is decreased. On these time scales, this blend does not fully relax in this temperature range.

B290 has been tacticity-matched to ePP and thus has a similar potential to crystallize. DSC measurements, discussed below, show that B290 has a higher degree of crystallinity than ePP. Thus the B290 should experience a greater effect from crystallite fillers. Modeling B290 as a system with noninteracting filler particles is oversimplified, however, for this model does not predict the absence of crossover behavior. At this level of isotacticity the crystalline regions may interact, leading to more complex relaxation behavior. Relaxation may take place on time scales longer than were employed in these oscillatory experiments. For purposes of comparison, eq 3 is used to calculate a length of chains between equivalent point constraints, M_{pc}, for B290. G°_N at 25 °C is 1.5 × 10^6 Pa for this sample. Accounting for the difference in density between atactic and isotactic PP, ρ is calculated on the basis of the [mmmm] of the sample using density values found in the literature (880 kg/m^3).[28] B290 was found to have an M_{pc} of 1470. This corresponds to an average value of 35 monomers between point constraints. This is a less constrained network than ePP, which had 21 monomers between point constraints by eq 3.

The rheology of the ePP solvent fractions was studied to probe the effect of compositional heterogeneity on the ePP sample. The solvent fractions of ePP demonstrate a variety of mechanical behavior. The rheological behavior of ES ([mmmm] = 0.18) resembles that of aPP, showing good time−temperature superposition across the entire frequency and temperature range probed. With the plateau of G' at 25 °C (5.4 × 10^5 Pa) and eq 3 above, M_{pc} was estimated to be 3990 for ES, which is similar to the entanglement molecular weight found for the atactic sample. Thus, this fraction shows no appreciable rheological difference from the atactic polymer tested.

The rheology of the heptane-soluble fraction (HS) ([mmmm] = 0.33) shows that mechanically the HS resembles ePP. This fraction matches the tacticity of the ePP parent sample and of the homopolymer blend B290 discussed above. Moduli for the HS collected at low temperatures are discontinuous and offer poor time−temperature superposition for data below 115 °C. Data collected at 145, 180, and 200 °C show good time−temperature superposition and approach good terminal behavior. With the plateau of G' at 25 °C (2.2 × 10^6 Pa) and eq 3, M_{pc} was estimated to be 990 for the HS, which translates to an average length between point constraints of 24 monomers.

The heptane-insoluble fraction (HI) ([mmmm] = 0.51) quasi-master curve shows that, at 115 °C and below, the HI behaves like an elastic solid, with frequency independent moduli and a dominant storage modulus. At 145 °C the sample reveals a step decrease in the elastic modulus. HI data taken at 160, 180, and 200 °C show good time−temperature superposition. At these higher temperatures the sample is able to relax and approaches terminal flow behavior.

The elastomeric polypropylene ePP, B290, and HS all have the same potential to crystallize by NMR. DSC results, which are discussed in detail below, show that at 25 °C B290 has the largest crystalline filler content (14.4% crystalline), followed by ePP (12.4% crystalline), and finally the HS (5.2% crystalline). Despite this lower filler content, rubber elasticity theory and small amplitude rheology reveal that there are fewer monomers between equivalent point constraints for ePP and the HS than for B290, showing that these systems form a more constrained network. Evidently, the ePP and HS crystallites form different physical constraints than the B290 system. These differences in the thermal character motivate an analysis of the formation and persistence of the crystallites found in these systems.

Thermal Behavior. The crystallization and melting behavior of the elastomeric polypropylenes and the homopolymer blends were investigated by differential scanning calorimetry (DSC). DSC data from ePP, its solvent fractions, the homopolymers, and homopolymer blends are presented in Table 3.

Under the experimental conditions examined, ePP exhibits a single crystallization transition at T_c = 62 °C with a ΔH_c = −11 J/g. Upon heating, this elastomeric sample shows a broad melting transition that spans the temperature range from approximately 30 to 145 °C (Figure 5), the same temperature range over which time−temperature superposition failed. The elastomeric polypropylene ePP has a peak T_m of 142 °C and a ΔH_f of 26 J/g. A percent crystallinity, ϕ_c, for ePP

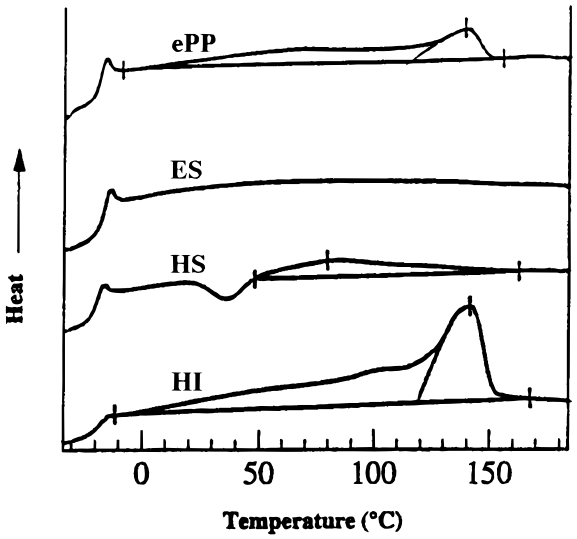

Figure 5. Differential scanning calorimetry (DSC) endotherms from the heating run at 20 °C/min. The bottom three curves are the solvent fractions, from top to bottom, ES, HS, and HI.

Table 3. Thermal Characterization

		cooling study		heating study		
sample	[mmmm]	T_c (°C)	ΔH_c (J/g)	T_m (°C)	ΔH_f (J/g)	$\Delta(\Delta H)$
ePP	0.32	62	−11	142	26	15
ES	0.18		0		0	0
HS	0.33		0	81	11	11
HI	0.51	85	−34	142	72	38
aPP	0.10		0		0	0
iPP290	0.92	109	−100	158	100	0
iPP41	0.85	94	−75	132	75	0
iPP16	0.84	84	−74	122	75	0
B290	0.33	90	−30	156	30	0
B41	0.31	74	−24	126	24	0
B16	0.30	69	−19	116	19	0

can be calculated from the following relation:

$$\phi_c = \frac{\Delta H_f}{\Delta H^e_{f,iPP}} \times 100\% \qquad (5)$$

where $\Delta H^e_{f,iPP}$ is the equilibrium heat of fusion for isotactic polypropylene (209 J/g). For ePP, $\phi_c = 12.4\%$.

Each of the solvent fractions of ePP exhibit distinct thermal behavior. The ether-soluble fraction (ES) behaves like the atactic homopolymer, showing no thermal transition upon cooling or heating under these experimental conditions. The heptane-soluble fraction (HS) shows no thermal transition upon cooling under these experimental conditions. Interestingly, upon heating, the HS demonstrates a crystallization exotherm at 37 °C and then a low-temperature melt endotherm at 81 °C with a ΔH_f of 11 J/g (Figure 5). When this sample was cooled and held at 25 °C for 12 h before the heating run, the crystallization exotherm disappears and only a broad melt endotherm is observed. The unaged HS sample has a $\phi_c = 5.2\%$. The heptane-insoluble fraction (HI) has a T_c of 85 °C and a ΔH_c of −34J/g. The HI fraction also exhibits a broad melting transition with T_m of 142 °C and a ΔH_f of 72 J/g. The HI fraction has a $\phi_c = 34.4\%$. Interestingly, the enthalpy of fusion of the ePP sample is higher than the sum of the enthalpies of its individual components for samples crystallized under these conditions. A weighted sum of the components ($\Delta H_{f,total} = 0.36[0\%] + 0.43[5.2\%] + 0.21[34.4\%]$) yields $\phi_{c,sum} = 9.4\%$ versus a $\phi_c = 12.4$ J/g for ePP. This increase in enthalpy upon combining fractions could be due to both a cocrystallization of more isotactic fractions with lower isotactic fractions as well as a shift in the kinetics of crystallization.

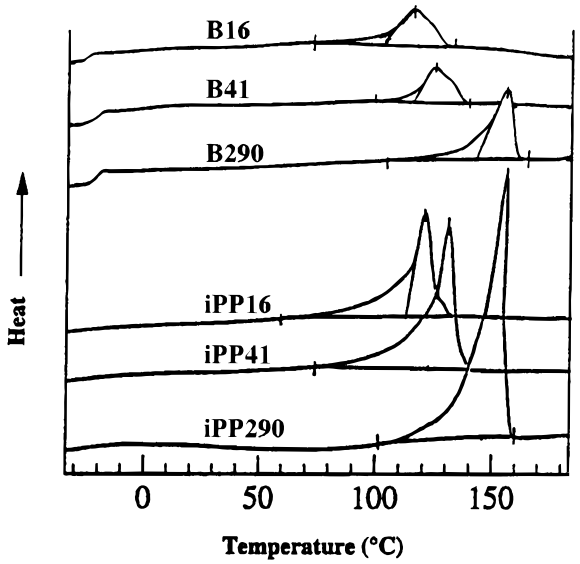

Figure 6. Differential scanning calorimetry (DSC) endotherms from the heating run at 20 °C/min. The bottom three curves are from isotactic homopolymers, from bottom to top, iPP290, iPP41, and iPP16. The top three curves are from the atactic/isotactic blends, from bottom to top, B290, B41, and B16.

The behavior of ePP and its solvent fractions is significantly different from that of isotactic homopolymers or from atactic/isotactic blends. The three isotactic homopolymers all revealed a single, sharp crystallization transition. iPP290, iPP41, and iPP16 have T_c values of 109, 94, and 84 °C, respectively. The ΔH_c of iPP290 is the largest in magnitude (−100 J/g), followed by iPP41 (−76 J/g), and iPP16 (−74 J/g). The melt behavior of the isotactic homopolymers is shown in Figure 6. In contrast to the broad melt transition for ePP, these heating experiments reveal well-defined thermal transitions for the three isotactic samples. iPP290 exhibits the highest melting temperature (T_m = 158 °C, ΔH_f = 100 J/g), followed by iPP41 (T_m = 132 °C, ΔH_f = 76 J/g) and iPP16 (T_m = 122 °C, ΔH_f = 74 J/g).

The thermal behavior of the blends mimic the behavior seen in their parent homopolymers. The T_c and T_m are highest and the magnitudes of ΔH_c and ΔH_f are largest for B290, followed by B41, and then B16. B270 has the largest ϕ_c (14.4 J/g) followed by B41 (11.5%) and B16 (9.1%). Figure 6 also shows that all three blend samples exhibit distinct melting endotherms. A distinct melt transition is consistent with the existence of time−temperature superposition above and below 160 °C for B290.

Comparison of the crystallization and melt enthalpies shows further differences between the blends and the elastomeric samples. In our experiments the homopolymers and homopolymer blends exhibit heats of crystallization and fusion of equal magnitude whereas in ePP and its fractions $|\Delta H_c| < |\Delta H_f|$. The $\Delta[\Delta H]$ ($\equiv |\Delta H_f| - |\Delta H_c|$) for ePP, HS, and HI is 15, 11, and 38 J/g, respectively, whereas the $\Delta[\Delta H]$ is zero for the homopolymers and homopolymer blends.

This difference in experimental measurements of crystallization and melting of ePP and its fractions

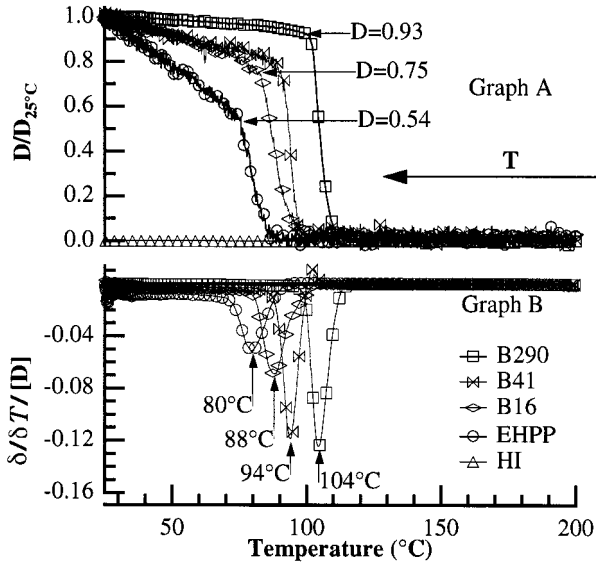

Figure 7. (A) Trace of depolarized intensity data from cooling experiments for systems that have an [mmmm] = approximately 0.30. (B) $\delta/\delta T$[depolarized intensity] data from cooling experiments for systems that have an [mmmm] = approximately 0.30. Data points indicate every fifth point.

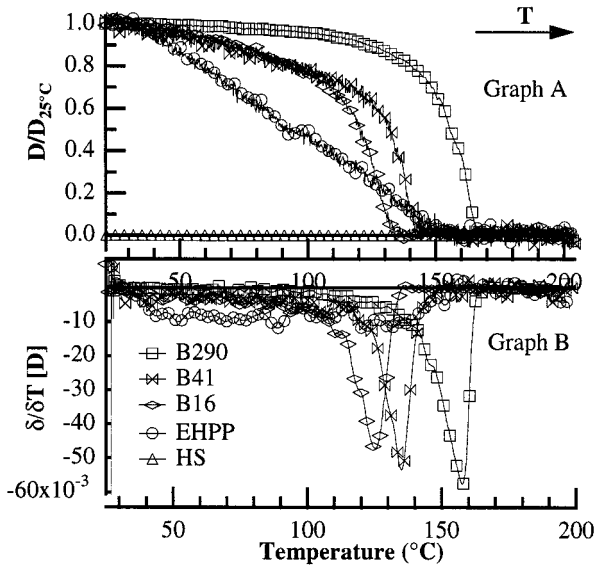

Figure 8. (A) Trace of depolarized intensity data from heating experiments for systems that have an [mmmm] = approximately 0.30. (B) $\delta/\delta T$[depolarized intensity] data from heating experiments for systems that have an [mmmm] = approximately 0.30. Data points indicate every fifth point.

prompted us to study the kinetics of crystallization by polarizing microscopy.[30−32] This technique measures the intensity of light transmitted through crossed polarizers as a function of the growth of birefringent crystalline regions. Systems that exhibit Avrami kinetics will crystallize rapidly over a narrow temperature range as they are cooled below their T_c.[33] This results in an increase in the number of crystalline regions that are of the appropriate length scale to be detected by this depolarization technique. The growth of these birefringent crystalline regions causes a rapid increase in the depolarized intensity over the same narrow temperature range, ideally followed by a plateau that marks the end of crystallization. The crystallization temperature can be determined from the maximum rate of growth of depolarization, $T_{dep,c}$. This technique was chosen because it is sensitive to small-length-scale birefringent regions (~0.5 μm)[34] and because the fast response time of photodiodes allowed us to monitor the rapid crystallization that occurs near T_c.

Shown in Figure 7A is the trace of the depolarized intensity data plotted against temperature collected during cooling experiments. The figure contains data from B290, B41, B16, ePP, and the HS, which all have ^{13}C NMR [mmmm] = approximately 0.30. To compare rate information, each data set has been normalized to the depolarization value at 25 °C. The data reveal that there are two crystallization regimes: an initial fast crystallization and a secondary slower crystallization. The tacticity-matched samples differ in initial temperature of crystallization ($T_{dep,c}$), rate of initial crystallization, and the distribution of crystallization that occurs in the two regimes. Figure 7A shows that B290 has the highest $T_{dep,c}$ (104 °C), followed by B41 (94 °C), B16 (88 °C), and ePP (80 °C). HS shows no depolarization under these conditions. The rate of initial crystallization is shown in Figure 7B, which plots ($\delta/\delta T$)[depolarization] as a function of temperature. Figure 7B shows that B290 has the initial crystallization rate of greatest magnitude (−0.13 °C^{-1}), followed by B41 (−0.12 °C^{-1}), B16 (−0.07 °C^{-1}), and ePP (−0.05 °C^{-1}). Figure 7A shows that B290 carries out 95% of its crystallization in this rapid regime. Both B41 and B16 performed 75% of their crystallization in the initial crystallization regime, whereas only 50% of ePP crystallized by the end of its rapid growth phase. After this initial rapid growth, all samples show a relatively linear increase in depolarized intensity as they are cooled to 25 °C. Thus, depolarization data indicate that half of ePP crystallization occurs in this secondary slow growth regime.

Figure 8A shows the depolarization data collected from heating experiments for the same set of samples. These data show large differences between the melt behavior of the blend systems and ePP. Data for the blends illustrate a sharp depolarization roll-off temperature, $T_{dep,m}$. B290, B41, and B16 possess a $T_{dep,m}$ of 161, 137, and 127 °C, respectively. In contrast, ePP shows a steady linear decrease in depolarized intensity over a temperature range from 42 to 147 °C, reflecting the differences seen in the DSC and rheology measurements. The HS shows no thermal transition under these conditions. The inability of the HS sample to depolarize light is striking, given that DSC results show that this sample can crystallize. Even after several months, the HS sample shows no depolarization of light. As the depolarization technique probes length scales on the order of wavelength of light (0.63 μm), the HS crystallite must be small compared to this length scale.

The crystallization behavior of the HI fraction is qualitatively similar to that of the ePP parent sample, despite having a larger isotacticity ([mmmm] = 0.51). For comparison, the trace of the depolarization data of the HI is presented in Figure 9 overlaying the data from ePP and the blends from Figure 7. The HI has a $T_{dep,c}$ of 100 °C. After the initial rapid crystallization regime, the HI only achieved 56% of its final depolarization value, after which it shows a similar linear growth in depolarization as the other samples. Heating the sample reveals that, like ePP, the depolarized intensity decreases without a distinct roll-off over a temperature range from 40 to 147 °C.

The large differences in thermal behavior between the elastomeric sample and atactic/isotactic blends reveals

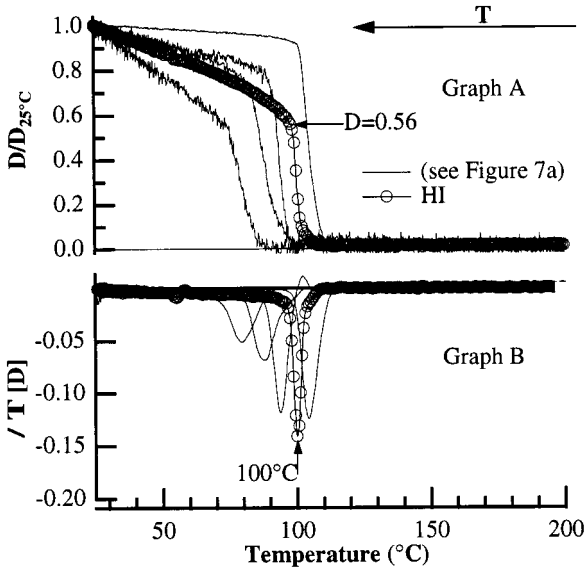

Figure 9. (A) Trace of depolarized intensity data from cooling experiment for the heptane-insoluble fraction (HI) overlaid on data from systems that have an [mmmm] = approximately 0.30. (B) $\delta/\delta T$[depolarized intensity] data from heating experiments for the heptane-insoluble fraction (HI) overlaid on data from systems that have an [mmmm] = approximately 0.30. Data points indicate every fifth point.

that the ^{13}C NMR [mmmm] pentad is a poor predictor of crystallization behavior. The elastomeric ePP sample may crystallize and melt differently than the blends as a consequence of thermodynamics of crystallite formation and/or as a consequence of the kinetics of crystallization, preventing the sample from achieving its optimal morphology. Generally, polymer crystallization is a kinetically driven phenomenon in which lower temperatures favor the thermodynamics of forming nuclei while higher temperatures favor increased diffusion.[35] It is the balance of these process that determines how a sample will crystallize and melt.

The slower rate of crystallization appears to correlate with the increase in the defect concentration of the isotactic segments. The isotactic homopolymers studied differ in M_w, stereoregularity, and regioerror density. Galante et al. assert that M_w has a minimal effect on polypropylene crystallization compared with defect concentration.[14] DSC and depolarization results show that as the stereo- and regioerrors of the isotactic samples increase, the T_c values decrease. Galante et al. attribute the lower T_c values of the metallocene isotactic samples to a higher interfacial surface free energy, σ_e, arising from the greater number of stereo- and regioerrors in the metallocene systems. Tacticity-matched blends formed from these homopolymers reproduce this trend. However, the reduction in T_c and $T_{c,dep}$ is even more pronounced in the ePP sample. This could indicate a higher σ_e in the ePP crystallites due to a microstructure capable of holding more noncrystallizable species close to the crystallite surface.

The differences in diffusion and mobility of various segments may also affect the kinetics of crystallization. The secondary crystallization regime revealed by the depolarization experiments may result from a diffusion limitation cause by an accumulation of structural defects at the crystallite surface. In the tacticity-matched samples, the amount of crystallization occurring in this slow regime increases with increasing isotactic defect concentration. Half of the ePP crystallization occurs in this slower regime, indicating a strong kinetic limitation. Crystallization differences could be the result of an atactic/isotactic multiblock microstructure tethering atactic segments to a crystallite surface; however, these experiments are not able to directly determine the origin of kinetic differences.

The heating experiments reveal that ePP and its solvent fractions experience a much broader range of thermal transitions than the homopolymer blends. This breadth shows that the ePP crystallites are able to melt, re-form, and anneal over a wide temperature range, and thus they form a much different network than the blend systems. These annealing crystallites manifest themselves in a temperature-dependent elastomeric response, as seen in the oscillatory rheological measurements described above.

Conclusions

Elastomeric polypropylene prepared with a bis(2-phenylindenyl)zirconium dichloride catalyst is a material compositionally heterogeneous in tacticity. Physical property data show that ePP is an elastomer at room temperature. Small amplitude rheological investigations reveal that elastomeric polypropylenes possess temperature-dependent physical networks in which the applied stress does not relax on the time scale of the experiment. Comparison with an atactic/isotactic blend also shows that the plateau modulus G_N° may not be appropriate for estimating the amorphous segment length in a stereoblock structure. The homopolymer blend system also exhibits a plateau modulus indicative of a constrained sample. Recent rheo-optical studies of step-shear responses show that blend systems do relax on very long time scales, while ePP systems maintain a high degree of stress and do not completely relax after the application of strain.

Thermal studies show that the crystallites essential to the ePP elastomeric network differ significantly from that of tacticity-matched atactic/isotactic polypropylene blends. Elastomeric polypropylene and its solvent fractions display slower crystallization kinetics than the tacticity-matched homopolymer blends. The prominence of a second, slower crystalline regime for the ePP sample may indicate that crystallization becomes mass diffusion limited. In addition, ePP, a mixture of the ES, HS, and HI, crystallizes faster than the HS yet possesses the same [mmmm]. This suggests that the presence of more highly isotactic fractions facilitates the crystallization of these samples. Therefore, isotactic polypropylene might prove to be a useful nucleating agent for elastomeric polypropylenes. Further studies are in progress to evaluate this possibility. Clearly, ^{13}C NMR [mmmm] measurements do not offer a simple predictor of crystallization behavior.

Acknowledgment. E.D.C. acknowledges the National Science Foundation for Graduate Fellowship support. G.G.F. acknowledges the National Science Foundation (NSF DMR 9522642-001) for financial support. R.M.W. acknowledges Amoco Chemical Co., the NSF (NSF DMR 9528636-002), and the Center for Polymeric and Interfacial Macromolecular Assemblies (CPIMA) for financial support. We would also like to thank Amoco Chemical Co. for providing the elastomeric sample and the molecular weight data and M. D. Bruce, E. Hauptman, and L. Resconi for the preparation of the atactic and isotactic polypropylene homopolymer samples.

Finally, we would like to thank Dr. Sai Kumar for discussions on the polarization experiments and S. Lin for her help in determining regioerror concentrations.

References and Notes

(1) *Thermoplastic Elastomers: A Comprehensive Review*; Legge, N. R., Holden, G., Schroeder, H. E., Eds.; Hanser Verlag: New York, 1988.
(2) Natta, G.; Mazzanti, G.; Crepsi, G.; Moraglio, G. *Chim. Ind. (Milan)* **1957**, *39*, 275−283.
(3) Natta, G. *J. Polym. Sci.* **1959**,*34*, 531−549.
(4) Natta, G.; Crespi, G. U.S. Patent 3,175, 999, 1965.
(5) Ziegler, K.; Holzkamp, H.; Martin, H. *Angew. Chem.* **1955**, *67*, 541−547.
(6) Ziegler, K. *Angew. Chem.* **1964**, *76*, 545.
(7) Collette, J. W.; Tullock, C. W. (E. I. du Pont de Nemours). U.S. Patent 4,335, 225, 1982.
(8) Collette, J. W.; Tullock, C. W.; MacDonald, R. N.; Buck, W., H.; Su, A. C. L.; Harrel, J. R.; Mulhaupt, R.; Anderson, B. C *Macromolecules* **1989**, *22*, 3851−3858.
(9) Collette, J. W.; Overnall, D. W.; Buck, W. H.; Ferguson, R. C. *Macromolecules* **1989**, *22*, 3858−3866.
(10) Llinas, G. H.; Dong, S.-H.; Mallin, D. T.; Rausch, M. D.; Lin, Y.-G.; Winter, H. H.; Chien, J. C. W. *Macromolecules* **1992**, *25*, 1242−1253.
(11) Mallin, D. T.; Rausch, M. D.; Lin, Y.-G.; Dong, S.; Chien, J. C. W. *J. Am. Chem. Soc.* **1990**, *112*, 2030−2031.
(12) Chien, J. C. W.; Llinas G. H.; Rausch, M. D.; Lin, G. Y.; Winter, H. H. *J. Am. Chem. Soc.* **1991**, *113*, 8569−8570.
(13) Coates, G. W.; Waymouth, R. M. *Science* **1995**, *267*; 217−219.
(14) Galante, M. J.; Mandelkern L.; Alamo, R. G.; Lehtinen, A.; Paukkeri, R. *J. Therm. Anal.* **1996**, *47*, 913−929.
(15) Bruce, M. D. Ph.D. Dissertation, Stanford University, 1997.
(16) Resconi, L.; Fait, A.; Piemontesi, F.; Colonnesi, M.; Rychlichi, H.; Ziegler, R. *Macromolecules* **1995**, *28*, 6667−6676.
(17) Fuller, G. G. *Optical Rheometery of Complex Fluids*; Oxford: New York, 1995.
(18) Bovey, F. A. *High-Resolution NMR of Macromolecules*; Academic Press: New York, 1972.
(19) Bovey, F. A. *Chain Structure and Conformation of Macromolecules*; Academic Press: New York, 1982.
(20) Zambelli, A.; Locatelli, P.; Bako, G.; Bovey, F. A. *Macromolecules* **1975**, *8*, 687−689.
(21) Inoue, Y.; Itabashi, Y.; Chujo, R.; Doi, Y. *Polymer* **1984**, *25*, 1640−1644.
(22) Burfield, D. R.; Loi, P. S. T. *J. Appl. Polym. Sci.* **1988**, *36*, 279−293.
(23) Luongo, J. P. *J. Appl. Polym. Sci.* **1960**, *3*, 302−309.
(24) Brader, J. J. *J. Appl. Polym. Sci.* **1960**, *3*, 370−371.
(25) Physical properties of ePP are similar to other elastomeric polypropylenes: tensile strength = 9.3 MPa, elongation to break = 880%, tensile set at 300% elongation = 30−40%. Full details of these physical property tests will be reported elsewhere (Hu, Y.; Krejchi, M. T.; Shah, C.; Waymouth, R. M.; Myers, C. L. *Macromolecules*, submitted.
(26) Ferry, J. D. *Viscoelastic Properties of Polymers*, 3rd ed.; Wiley: New York, 1980.
(27) Lin, Y.-G.; Mallin, D. T.; Chien, J. C. W.; Winter, H. H. *Macromolecules* **1991**, *24*, 850−854.
(28) Brandrup, J.; Immergut, E. H. *Polymer Handbook*, 3rd ed.; Wiley: New York, 1989.
(29) Bachelor, G. K. *J. Fluid Mech.* **1970**, *41*, 545−570.
(30) Magill, J. H. *Polymer* **1961**, *2*, 221−233.
(31) Magill, J. H. *Polymer* **1962**, *3*, 35−42.
(32) Ding, Z.; Spruiell, J. E. *J. Polm Sci., Polym. Phys. Ed.* **1996**, *34*, 2783−2804.
(33) Avrami, M. *J. Chem. Phys.* **1941**, *9*, 177−184.
(34) Garetz, B. A.; Newstein, M. C.; Dai, H. J.; Jonnalagadda, S. V.; Balsara, N. P *Macromolecules* **1993**, *26*, 3151−3155.
(35) Keith, H. D.; Padden, F. J., Jr. *J. Appl. Phys.* **1964**, *35*, 1286−1296.

MA971106Q